JACS
JOURNAL OF THE AMERICAN CHEMICAL SOCIETY

ARTICLE

pubs.acs.org/JACS

Template Effect in the Competition between Haeckelite and Graphene Growth on Ni(111): Quantum Chemical Molecular Dynamics Simulations

Ying Wang,[†,∥] Alister J. Page,[‡,∥] Yoshio Nishimoto,[†] Hu-Jun Qian,[†] Keiji Morokuma,[*,‡,§] and Stephan Irle[*,†]

[†]Department of Chemistry, Graduate School of Science, Nagoya University, Nagoya 464-8602, Japan

[‡]Fukui Institute for Fundamental Chemistry, Kyoto University, Kyoto 606-8103, Japan

[§]Cherry L. Emerson Center for Scientific Computation and Department of Chemistry, Emory University, Atlanta, Georgia 30322, United States

Supporting Information

ABSTRACT: Quantum chemical molecular dynamics (QM/MD) simulations of ensembles of C_2 molecules on the Ni(111) terrace show that, in the absence of a hexagonal template or step edge, Haeckelite is preferentially nucleated over graphene as a metastable intermediate. The nucleation process is dominated by the swift transition of long carbon chains toward a fully connected sp^2 carbon network. Starting from a pentagon as nucleus, pentagons and heptagons condense during ring collapse reactions, which results in zero overall curvature. To the contrary, in the presence of a coronene-like C_{24} template, hexagonal ring formation is clearly promoted, in agreement with recent suggestions from experiments. In the absence of step edges or molecular templates, graphene nucleation follows Ostwald's "rule of stages" cascade of metastable states, from linear carbon chains, via Haeckelite islands that finally anneal to graphene.

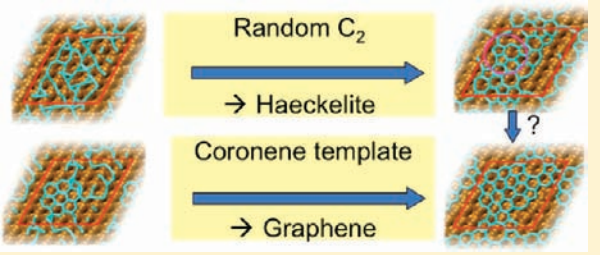

1. INTRODUCTION

Graphene exhibits remarkable electronic, optical, and mechanical properties.[1] This phenomenal material has therefore been ascribed a number of potential applications in electronic, spintronic, sensor, and mechanical devices. Its electronic properties depend explicitly on the edge structure,[2−4] which provides an additional control parameter[5] for the purpose of electronic or spintronic property tuning. Haeckelite, on the other hand, is a hypothetical planar carbon compound that is intrinsically metallic, irrespective of its edge structure. Haeckelite's structure can be formally derived from graphene by periodical replacement of hexagon pairs with pentagon/heptagon defects. It was discussed in a number of previous theoretical studies[6−10] but has never been experimentally synthesized and characterized thus far, and its formation mechanism is unknown. On the other hand, it is apparent that heptagon−pentagon pairs are major constituents of damaged or irradiated samples of graphene.[11,12]

In recent years, chemical vapor deposition (CVD) techniques have begun to dominate the field of graphene synthesis (see, e.g., refs 13,14). The CVD process is a highly optimized technique, and is already well established in the synthesis of many other nanostructures, most notably carbon nanotubes (CNTs).[15,16] In the case of graphene CVD synthesis, a number of different transition metals have proven to be catalytically active, with nickel being most commonly employed.[17−22] Despite practical advances in synthesis techniques resulting from phenomenological growth models, the atomistic mechanism by which graphene nucleates on catalyst surfaces remains the topic of fierce debate. It is clear that carbon solubility plays an important role: Ni generally has a higher C solubility than, for instance, Cu. The role of carbide formation is consequently well documented for Ni-catalyzed graphene synthesis,[17] whereas this is not so with respect to Cu.[23] Temperature is equally important: Lahiri et al.[24] reported low-temperature conversion of a surface carbide to graphene below 460 °C, while at higher temperatures carbon atoms[23] [for instance on Cu(111) or Ni(111)], C_2 units[25] [on Rh-YSZ-Si(111)], or linear carbon chains[26] [on Ir(111)] attach to graphene islands. Evidence was found that graphene sheet growth on Ni(111),[19,27] Ru(0001),[26] and Ir(111)[28] begins with carbon atoms adsorbed at step edge defects, while it appears that graphene islands nucleate spontaneously on terraces in the case of Ir(111),[28] Rh(111),[29] and Cu(111).[23] Undoubtedly, Smoluchowski ripening via carbon-island coalescence plays an important role in the graphene growth process.[28−30] Indeed, Wang et al. have recently identified actual coronene-like C_{24} units as dominant islands undergoing surface migration on Rh(111).[29] Although much work has been done, a systematic computational study investigating the role of metal−carbon binding energy, carbon solubility, carbide formation,

Received: July 12, 2011
Published: October 03, 2011

feedstock concentration, temperature, etc. for the formation mechanism of graphene on metal surfaces clearly is timely.

Previous theoretical investigations of graphene nucleation at step edges[31,32] or terraces[26,32,33] have either employed static models (thereby neglecting irreversible dynamic processes occurring during nonequilibrium growth), or captured only ultra short dynamics of individual C−C bond formation in density functional theory (DFT)-based molecular dynamics (MD) simulations.[34] We have therefore employed the quantum chemical MD simulations based on the computationally more economical self-consistent-charge density-functional tight-binding (SCC-DFTB) method.[35] A similar methodology was previously employed by us in the investigation of the nucleation mechanism of single-walled carbon nanotube (SWCNT) caps on C_2-covered Fe_{38} nanoparticles.[36] With a plethora of different growth scenarios described in the experimental literature, an atomistic MD study needs to focus on a certain aspect of the growth mechanism. To this end, we concentrated on the nucleation of the first sp^2 carbon ring systems from C_2 molecules on a terrace, at a constant and rather large 83.3 mol % of the carbon density of a perfect monolayer coverage of the metal surface by a continuous sheet of graphene. Lower concentrations did not yield any significant amount of sp^2 network on time scales feasible for computer simulations. As will be presented in section 3, we find that only Haeckelite spontaneously nucleates as the result of a "pentagon-first" mechanism, and that a template effect can be used to promote the direct formation of a hexagonal graphene carbon network.

2. COMPUTATIONAL METHODOLOGY

All calculations were carried out using the DFTB+ program.[37] The SCC-DFTB wave function, energy, and gradient were computed "on-the-fly" at each step of the dynamics. A fractional orbital occupation Fermi−Dirac distribution was employed with an electronic temperature (T_e)[38,39] of 3000 K. This approach alleviated the convergence issues that arose from the presence of many near-degenerate Ni d orbitals and unterminated C bonds, and has been used by us previously in the context of transition-metal catalyzed single-walled CNT (SWCNT) nucleation and growth.[40,41] It is noted here that T_e = 3000 K is the highest temperature at which the crystalline features of the Ni(111) surface were maintained. At higher values of T_e (up to 10 000 K) significant deformation of the upper atomic layers in the Ni(111) slab was observed. The equations of motion of nuclei were integrated using the Velocity−Verlet algorithm,[42] with the NVT ensemble being maintained via a Nosé−Hoover chain thermostat (chain-length 3)[43] connected to the degrees of freedom of the system. The nuclear temperature was maintained at 1180 K throughout all simulations. The accuracy of the transition metal−carbon DFTB parameters employed here have themselves been verified previously.[44,45] The use of these Ni−C parameters yields absolute errors (with respect to the B3LYP/SDD+6-31G(d) level of theory) in bond lengths, bond angles, and dissociation energy barriers on the order of 0.01−0.1 Å, 5−10°, and 10−20 kcal/mol, respectively. It has been shown in several prior investigations[4,46] that inclusion of multireference effects in the quantum chemical method is crucial in the description of small carbon clusters, such as acene chains and sheets. The DFTB method itself is effectively a second order approximation to density functional theory, and consequently multireference effects are only approximately considered using a finite T_e. However, we anticipate, in the present context, the quantum chemical method employed to be secondary in determining the formation dynamics compared to other, more pertinent factors such as temperature, carbon concentration, and the presence of a metal catalyst.

The four-layer Ni(111) model surface used in both models consisted of 144 Ni atoms. Three-dimensional periodic boundary conditions (PBC) were enforced on this model system during all simulations. Adjacent Ni(111) surfaces were separated by a vacuum region of 10 nm. Our treatment of PBC employed the Γ-point approximation (supplementary simulations with increased *k*-point sampling showed that such a sampling scheme was sufficient for this Ni(111) structure). The SCC-DFTB optimized *a*, *b*, and *c* distances of this model surface were 1.245, 1.245, and 0.652 nm, respectively. To study the role of the template effect on graphene nucleation, we set up two different carbon-containing model systems, named H and G systems. Ten replica trajectories were run for both G and H models, labeled as l_h-10_h and 1_g-10_g, respectively. The H model system consisted of 30 C_2 moieties adsorbed in randomly chosen positions with randomly selected orientations onto 10 pristine Ni(111) surfaces, randomly chosen from the last 5 ps of a 10 ps annealing of this surface. This model system is a two-dimensional analogy to our earlier study of fullerene formation.[47] Each C_2 species was placed ca. 2.5 Å above the surface. The G model system consisted of 18 C_2 moieties adsorbed onto an optimized Ni(111)−C_{24} complex, where "C_{24}" was a coronene-like carbon skeleton without hydrogen atoms. The 18 C_2 were randomly placed surrounding the C_{24} unit. The present models ensure that the total carbon densities were the same in both systems (60 C). As noted previously, this is equivalent to 83.3 mol % of pristine monolayer graphene, which brings into question the influence of the carbon concentration on the nucleation mechanism itself. In that sense, the initial conditions employed here are certainly somewhat too high. However, without a step edge, we found that lower carbon concentrations do not allow nucleation of sp^2 polygonal networks, at least on the time scales employed in the present simulations. The initial velocities of the atoms in each individual trajectory were chosen randomly, satisfying a Maxwell−Boltzmann distribution corresponding to 1180 K. In order to study the dynamics and mechanism of nucleation,

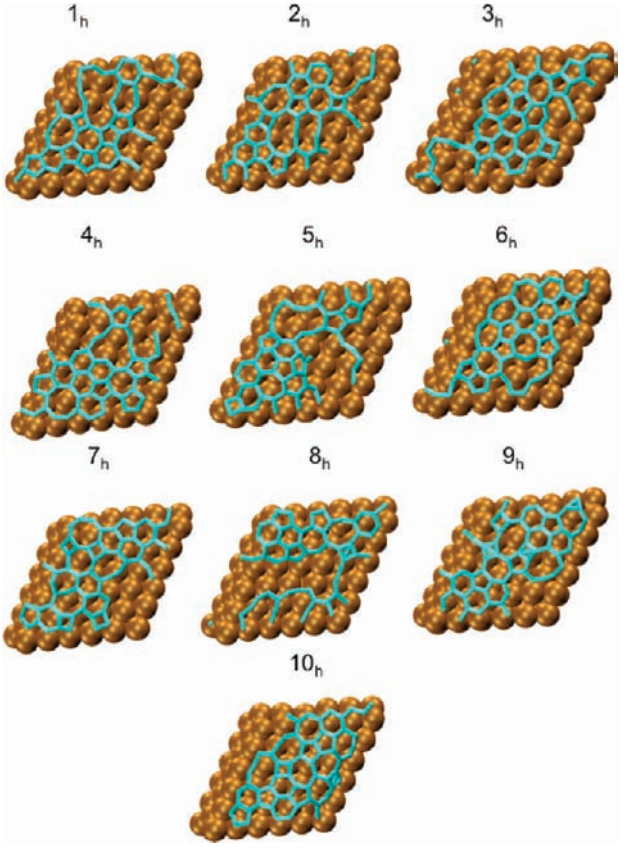

Figure 1. Geometries of trajectories 1_h-10_h following 50 ps SCC-DFTB/MD simulation.

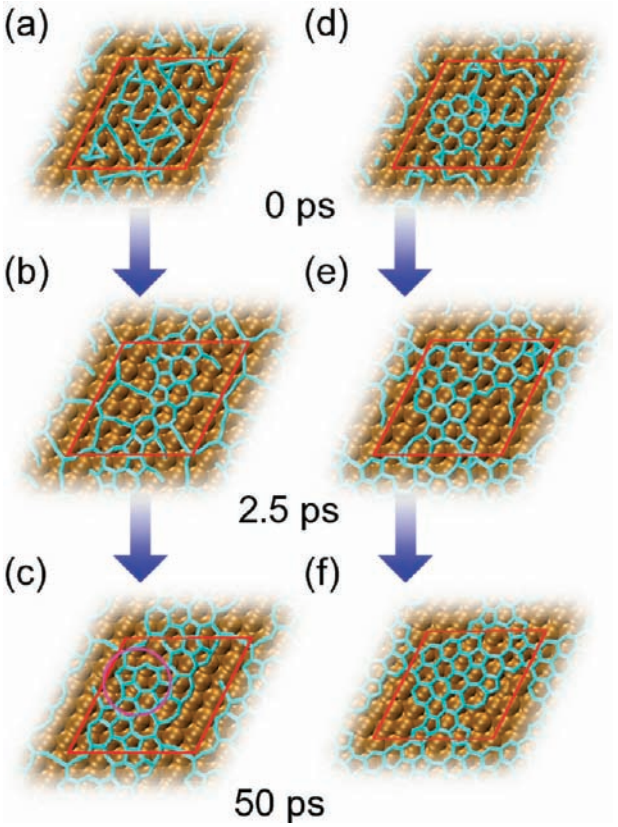

Figure 2. Snapshots of trajectories 6_h (a−c, left, Haeckelite) and 7_g (d−f, right, graphene) at 0, 2.5, and 50 ps, respectively. The location of the periodic boundary is indicated by the red line. The circle in part c denotes an area of late ring collapse from a Y-junction.

these initial structures for both models were annealed further in production runs at 1180 K for a period of 50 ps. The initial structures of trajectories 1_h-10_h and 1_g-10_g are given in Figures S1 and S2, respectively (note that prefix S indicates material given in the Supporting Information).

3. RESULTS AND DISCUSSION

We will first discuss the reaction observed in the C_2-only H model system. The structures of trajectories 1_h-10_h following 50 ps of SCC-DFTB/MD simulation are depicted in Figure 1. Apparently, and somewhat surprisingly to us at first, many defects such as four-, five-, six-, seven-, and even eight-membered rings formed. Among these defects, 5−7 Thrower−Stone−Wales defects are most frequently observed. Here taking trajectory 6_h as a reprehensive trajectory, we show the snapshots at 0, 2.5, and 50 ps in Figure 2a−c. Trajectory 6_h is also featured in Movie S1. The average populations of polygonal carbon rings observed in trajectories 1_h-10_h are shown in Figure 6a as a function of time (ring populations of individual trajectories 1_h-10_h are provided in Figure S3). It is immediate from these figures that the high density of the C_2 units initiated spontaneous sp carbon chain formation, which was followed by an almost instantaneous interchain reactive networking process during the first 2.5 ps of annealing. Following this initial period of "reactive network formation" was a more subdued period of annealing. The majority of carbon rings that were generated after 50 ps were formed within the first 5 ps of simulation, although occasional ring isomerizations are evident also at later stages in individual

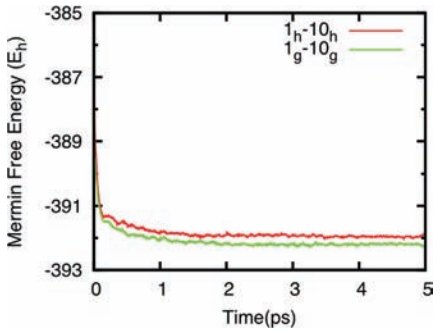

Figure 3. Average Mermin free energy during the first 5 ps of graphene and Haeckelite nucleation. All data averaged over 10 trajectories, respectively. Following this period, the latter system is on average ca. 0.1 eV higher in energy per carbon atom compared to graphene. This indicates that such Haeckelite systems are potentially metastable structures formed during graphene nucleation.

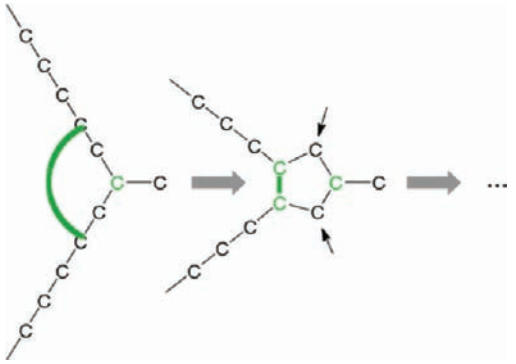

Figure 4. Schematic depiction of sp to sp^2 carbon conversion via the pentagon-first mechanism, the initial stage of carbon network nucleation. Black arrows indicate intermediate divalent carbon atoms possessing unpaired σ-electrons.

trajectories. The carbon chain and network formation was highly exothermic, as can be seen in the average Mermin free energy of trajectories 1_h-10_h (Figure 3). In the case of trajectory 6_h, this very reactive period lasted not much longer than 0.5 ps. After this period of C_n formation, Figure 2a−c shows that carbon ring formation proceeded via the interaction of adjacent linear chains on the Ni(111) surface. The presence of a Y-shaped junction, formed between two adjacent carbon chains, preceded the majority of ring formation events observed in this work. The motion of the "branches" of this junction structure, driven by the diffusion of the constituent carbon atoms on the Ni(111) terrace, then initiated the ring formation process. Figure 2b,c shows an explicit example of this process between 2.5 and 50 ps. In this case, a single Y-junction was generated at 2.5 ps. Its subsequent collapse to a pentagon, and its subsequent interaction with neighboring linear carbon chains, culminated in the formation of a conjugated 6−5−5−7 carbon ring structure (i.e., adjoined 6-, 7-, and two 5-membered carbon rings). Ultimately, after 50 ps the structure annealed to one in which only a single hexagon was observed. In effect, therefore, the structure thus formed was almost a pristine sheet of a pentagon-heptagon-rich Haeckelite.

This ring formation mechanism, depicted schematically in Figure 4, resembles closely the SWCNT cap nucleation mechanism on transition metal nanoparticles,[36,40,41] as well as the initial

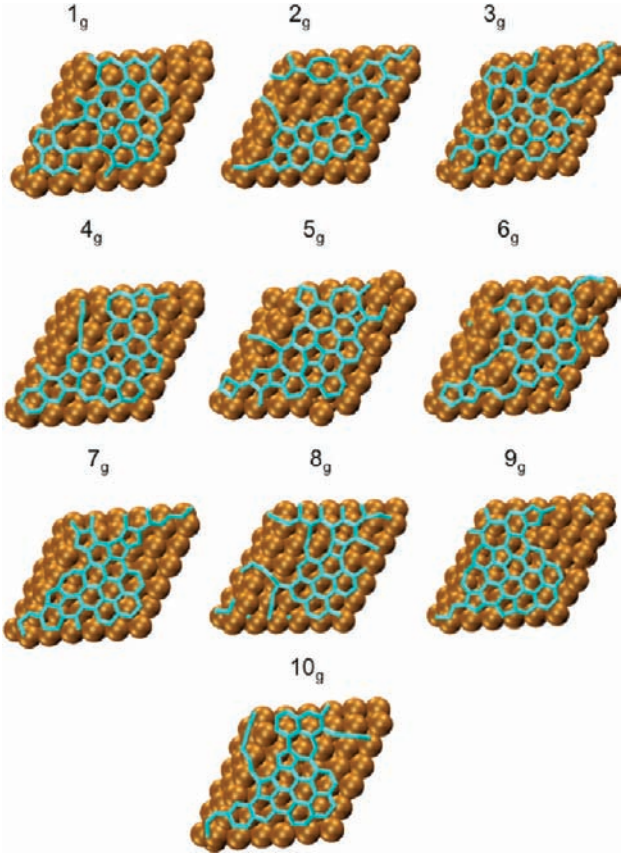

Figure 5. Geometries of trajectories 1_g-10_g following 50 ps SCC-DFTB/MD simulation.

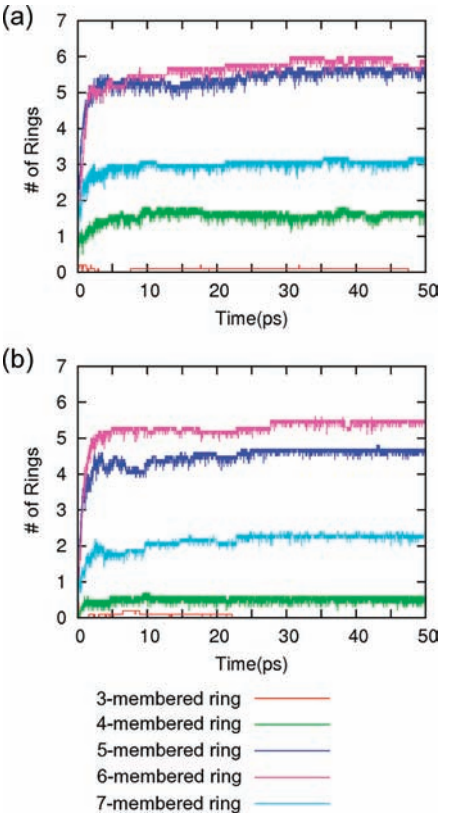

Figure 6. Average populations of newly formed carbon rings during 50 ps SCC-DFTB/MD simulation for (a) trajectories 1_h-10_h and (b) trajectories 1_g-10_g.

steps of fullerene nucleation from carbon chains.[48,49] This is despite the use of a different active precursor (C_2) in the present work: our previous simulations of SWNT nucleation from Fe-/Ni-carbide nanoparticles,[50] in which the precursor carbon was effectively atomic carbon, yielded an identical mechanism to that presented here. Notably, all observed sp^2 carbon network nucleation events begin with the formation of a Y-junction, which correspond in low carbon density situations to the C_4 "star configurations" described recently elsewhere.[33] Pentagon formation is driven by the motion of two Y-junction branches. However, the formation of an isolated pentagon is endothermic in vacuum by more than 1 eV. This endothermicity arises from the two divalent carbon atoms being forced to assume bond angles near 108°, leading to a change in hybridization from sp to sp^2, yet the dangling σ-bond pointing outside the pentagon remains (indicated by arrows in Figure 4). Although the analogous hypothetical pentagon formation process on a Ni(111) surface is equally endothermic due to the required surface deformation energy, the Ni−carbon interaction energy is enhanced by ca. 2 eV in comparison to the Y-junction. The effect of the metal on the stability of carbon structures during the nucleation process is therefore immediate. We note that surface Ni atoms partially move out of the surface to facilitate this stabilizing effect on the dangling carbon σ-bonds. Interestingly, the flat catalyst surface does not impede the formation of the initial pentagon, which usually introduces positive curvature into graphitic surfaces. Rather, on a flat surface, the positive curvature of the pentagon has to be compensated by an adjacent polygon with negative curvature. Heptagons associated with negative curvature are therefore the ideal polygonal shapes that are preferred in the immediate vicinity of a pentagon. Thus, the structures formed in trajectories 1_h-10_h resembled closely that of Haeckelite islands; i.e., they were composed predominantly of pentagons and heptagons. The curvature of the networked carbon structure was therefore effectively zero, and hence matched that of the flat Ni(111) surface.

We will now discuss the reaction observed in the template-containing G model system. The structures of trajectories 1_g-10_g following 50 ps of SCC-DFTB/MD simulation are shown in Figure 5. We find that with the coronene-like template more graphene-like structures (with less defects) are formed in comparison to the H model. We however also noticed that some coronene-like templates suffered outer ring transformation from six- to five-membered rings, such as those visible in trajectory 1_g, 2_g, 4_g, and 5_g. Since the final carbon coverage is ∼83 mol% instead of 100 mol%, there are still some polyene chains available for further ring formation. The rough time evolution of the representative trajectory 7_g is shown in Figure 2d−f. This trajectory is also featured in Movie S2. The average ring populations of newly formed polygonal carbon rings observed in trajectories 1_g-10_g as a function of time are shown in Figure 6b. Ring populations of individual trajectories 1_g-10_g are displayed in Figure S4. As was the case with trajectories 1_h-10_h, we found that the reaction resulting from C_2 adsorption in trajectory 7_g proceeded extremely rapidly. This fact is also reflected in Figure 6b, which shows the populations of polygonal carbon rings for trajectories 1_g-10_g. As was the case in the Haeckelite model systems, it was once

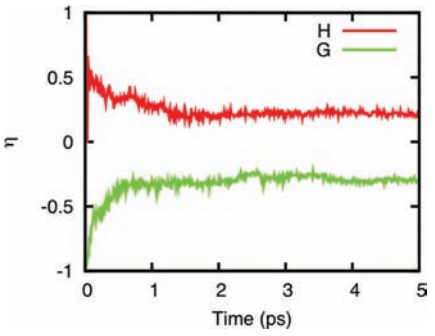

Figure 7. Average η observed during network nucleation in Haeckelite and graphene. All data averaged over trajectories 1_h-10_h, and 1_g-10_g, respectively.

again evident that the rapid ring formation mechanism was driven by the preceding formation of extended carbon chains on the Ni(111) surface. A comparison of Figure 6b with Figure 6a shows that the coronene-like fragment acted as a "template", which facilitated a more exclusive production of 6-membered rings at the expense of 5- and 7-membered rings, and significantly impeded the formation of 4-membered rings. In the case of trajectory 7_g, only a single defect ring (a heptagon) can be observed in the extended sp^2 carbon network after 50 ps. Since overall ring production was therefore reduced, the number of network-participating sp^2 carbon atoms at the final stage was smaller in the presence of the coronene-like fragment. It appears that the formation rate of Haeckelite islands is greater than that of graphene, at least under the present high carbon density conditions.

It is useful at this point to compare and contrast the structures generated in this work to "ideal" Haeckelite and graphene structures. We have done this via the dimensionless quantity, η, denoted as the "Haeckelite index"

$$\eta = \frac{n_5 + n_7 - n_6}{n_5 + n_7 + n_6} \quad (1)$$

where n_m are the numbers of m-membered rings in a sp^2 carbon network. For ideal graphene and Haeckelite structures, η is equal to -1 and $+1$, respectively. Thus, for an arbitrary sp^2-hybridized carbon network, η may vary continuously on $[-1, 1]$, and provides an indication as to the nature of the network. In particular, if η is positive, the structure is Haeckelite-like, whereas if η is negative, the structure is graphene-like. The computed average Haeckelite indices, $\langle\eta\rangle$, for the Haeckelite (H) and graphene (G) model systems during the period of reactive network formation are shown in Figure 7. Computed η for individual trajectories 1_h-10_h and 1_g-10_g are provided in Figures S5 and S6. The template effect of the coronene fragment on the carbon ring formation process is immediate from this figure, with $\langle\eta\rangle$ for trajectories 1_g-10_g suggesting that these structures are more graphene-like compared to those in trajectories 1_h-10_h. Comparison of the average Mermin free energy of both model systems, however, indicates that the formation of graphene, as opposed to Haeckelite, is an energetically more favorable process. For example, Figure 3 shows that, throughout the period of reactive network formation, the average Mermin free energy of the Haeckelite model system was larger than that of the graphene model system. Since stoichiometries of both model systems were identical, this comparison indicates that graphene is a more optimal structure compared to Haeckelite, as may be expected. We note that the difference in average Mermin free energies between G and H models is only about 0.1 eV, whereas this difference is far more pronounced between defect-free graphene and Haeckelite with roughly 0.3 eV.[8]

4. CONCLUSIONS

The present QM/MD simulations have shown that graphene nucleation begins with the formation of a pentagon from carbon chains, even on a perfect metal terrace. This result is surprising, counter to chemical intuition, and requires explanation: in response to the flat carbon distribution on a flat surface, carbon condenses initially in the form of a planar Haeckelite with alternating pentagon–heptagon structure. The free energy profiles of Figure 3 indicate that if the environmental temperature exceeds the kinetic barriers for Thrower–Stone–Wales transformations,[51] Haeckelite will eventually anneal to graphene. The time scale for Haeckelite to graphene transformation is probably rapid on experimental time scales, but dramatically exceeds the 50 ps time scale of the present MD simulations. Nevertheless, recent tight-binding Monte Carlo (MC) simulations[52] have reported precisely such annealing, since MC calculations avoid the problem of high energy barriers. The Haeckelite islands, nucleated in the absence of a hexagonal network, can therefore be interpreted as an intermediate metastable state, where graphene crystallization follows Ostwald's "rule of stages".[53] Since Haeckelite is intrinsically metallic, irrespective of its edge structure, our simulations suggest that it might be worthwhile experimentally to attempt its synthesis by depositing for instance hot polyynes on cold metal surfaces. Care should be taken that the metal surface remains free of hydrogen.

To the contrary, if a hexagonal seed nucleus is present among the carbon chains, such as coronene-like C_{24} islands that were recently identified experimentally by Wang et al.,[29] graphene growth proceeds in a more straightforward manner via the extension of the hexagonal lattice, and the graphene formation will involve less annealing via Thrower–Stone–Wales transformations. We therefore expect that high-quality graphene growth should dramatically benefit from the presence of hexagonal seed carbon clusters on the catalyst surface.

■ ASSOCIATED CONTENT

Supporting Information. Complete ref 27; snapshots of initial structures of all trajectories; movies of trajectories 6_h and 7_g; ring populations and Haeckelite indexes $\langle\eta\rangle$ for all trajectories. This material is available free of charge via the Internet at http://pubs.acs.org.

■ AUTHOR INFORMATION

Corresponding Author

morokuma@fukui.kyoto-u.ac.jp; sirle@iar.nagoya-u.ac.jp

Author Contributions

‖These authors contributed equally to this work.

■ ACKNOWLEDGMENT

This work was in part supported by a CREST (Core Research for Evolutional Science and Technology) grant in the Area of High Performance Computing for Multiscale and Multiphysics Phenomena from JST. S.I. acknowledges support by the Program for Improvement of Research Environment for Young Researchers

from Special Coordination Funds for Promoting Science and Technology (SCF) commissioned by the Ministry of Education, Culture, Sports, Science and Technology (MEXT) of Japan. A.J.P. acknowledges the Fukui Fellowship, Kyoto University. We are grateful for generous supercomputer time at the Institute for Molecular Science (IMS) in Okazaki, Japan.

REFERENCES

(1) Allen, M. J.; Tung, V. C.; Kaner, R. B. *Chem. Rev.* **2009**, *110*, 132.
(2) Son, Y.-W.; Cohen, M. L.; Louie, S. G. *Nature* **2006**, *444*, 347.
(3) Ritter, K. A.; Lyding, J. W. *Nat. Mater.* **2009**, *8*, 235.
(4) Pelzer, K.; Greenman, L.; Gidofalvi, G.; Mazziotti, D. A. *J. Phys. Chem. A* **2011**, *115*, 5632.
(5) Jia, X.; Campos-Delgado, J.; Terrones, M.; Meunier, V.; Dresselhaus, M. S. *Nanoscale* **2011**, *3*, 86.
(6) Crespi, V. H.; Benedict, L. X.; Cohen, M. L.; Louie, S. G. *Phys. Rev. B* **1996**, *53*, R13303.
(7) Terrones, H.; Terrones, M.; Hernandez, E.; Grobert, N.; Charlier, J. C.; Ajayan, P. M. *Phys. Rev. Lett.* **2000**, *84*, 1716.
(8) Rocquefelte, X.; Rignanese, G.-M.; Meunier, V.; Terrones, H.; Terrones, M.; Charlier, J. C. *Nano Lett.* **2004**, *4*, 805.
(9) Lusk, M. T.; Carr, L. D. *Phys. Rev. Lett.* **2008**, *100*, 175503.
(10) Lusk, M. T.; Carr, L. D. *Carbon* **2009**, *47*, 2226.
(11) Banhart, F.; Kotakoski, J.; Krasheninnikov, A. V. *ACS Nano* **2011**, *5*, 26.
(12) Kotakoski, J.; Krasheninnikov, A. V.; Kaiser, U.; Meyer, J. C. *Phys. Rev. Lett.* **2011**, *106*, 105505.
(13) Choi, W.; Lahiri, I.; Seelaboyina, R.; Kang, Y. S. *Crit. Rev. Solid State Mater. Sci.* **2010**, *35*, 52.
(14) Wei, D.; Liu, Y. *Adv. Mater.* **2010**, *22*, 3225.
(15) Cheng, H. M.; Li, F.; Su, G.; Pan, H. Y.; He, L. L.; Sun, X.; Dresselhaus, M. S. *Appl. Phys. Lett.* **1998**, *72*, 3282.
(16) Hafner, J. A.; Bronikowski, M. J.; Azamian, B. R.; Nikolaev, P.; Rinzler, A. G.; Colbert, D. T.; Smith, K. A.; Smalley, R. E. *Chem. Phys. Lett.* **1998**, *296*, 195.
(17) Shelton, J. C.; Patil, H. R.; Blakely, J. M. *Surf. Sci.* **1974**, *43*, 493.
(18) Nagashima, A.; Tejima, N.; Oshima, C. *Phys. Rev. B* **1994**, *50*, 17487.
(19) Grüneis, A.; Kummer, K.; Vyalikh, D. V. *New J. Phys.* **2009**, *11*, 073050.
(20) Chae, S. J.; Güneş, F.; Kim, K. K.; Kim, E. S.; Han, G. H.; Kim, S. M.; Shin, H.-J.; Yoon, S.-M.; Choi, J.-Y.; Park, M. H.; Yang, C. W.; Pribat, D.; Lee, Y. H. *Adv. Mater.* **2009**, *21*, 2328.
(21) Pollard, A. J.; Nair, R. R.; Sabki, S. N.; Staddon, C. R.; Perdigao, L. M. A.; Hsu, C. H.; Garfitt, J. M.; Gangopadhyay, S.; Gleeson, H. F.; Geim, A. K.; Beton, P. H. *J. Phys. Chem. C* **2009**, *113*, 16565.
(22) Odahara, G.; Ishikawa, T.; Otani, S.; Oshima, C. *e-J. Surf. Sci. Nanotechnol.* **2009**, *7*, 837.
(23) Li, X.; Cai, W.; Colombo, L.; Ruoff, R. S. *Nano Lett.* **2009**, *9*, 4268.
(24) Lahiri, J.; Miller, T.; Adamska, K.; Oleynik, I. I.; Batzill, M. *Nano Lett.* **2011**, *11*, 518.
(25) Müller, F.; Sachdev, H.; Hüfner, S.; Pollard, A. J.; Perkins, E. W.; Russell, J. C.; Beton, P. H.; Gsell, S.; Fischer, M.; Schreck, M.; Stritzker, B. *Small* **2009**, *5*, 2291.
(26) Loginova, E.; Bartelt, N. C.; Feibelman, P. J.; McCarty, K. F. *New J. Phys.* **2008**, *10*, 093026.
(27) Hofmann, S.; Sharma, R.; Ducati, C.; et al. *Nano Lett.* **2007**, *7*, 602.
(28) Lacovig, P.; Pozzo, M.; Alfe, D.; Baraldi, A.; Lizzit, S. *Phys. Rev. Lett.* **2009**, *103*, 166101.
(29) Wang, B.; Ma, X.; Caffio, M.; Schaub, R.; Li, W.-X. *Nano Lett.* **2011**, *11*, 424.
(30) Coraux, J.; N'Diaye, A. T.; Engler, M.; Busse, C.; Wall, D.; Buckanie, N.; Meyer zu Heringdorf, F.-J.; van Gastel, R.; Poelsema, B.; Michely, T. *New J. Phys.* **2009**, *11*, 023006.
(31) Saadi, S.; Abild-Pedersen, F.; Helveg, S.; Sehested, J.; Hinnemann, B.; Appel, C.; Nørskov, J. K. *J. Phys. Chem. C* **2010**, *114*, 11221.
(32) Gao, J.; Yip, J.; Zhao, J.; Yakobson, B. I.; Ding, F. *J. Am. Chem. Soc.* **2011**, *133*, 5009.
(33) Cheng, D.; Barcaro, G.; Charlier, J. C.; Hou, M.; Fortunelli, A. *J. Phys. Chem. C* **2011**, *115*, 10537.
(34) Wu, P.; Zhang, W.; Li, Z.; Yang, J.; Hou, J. G. *J. Chem. Phys.* **2010**, *133*, 071101/1.
(35) Elstner, M.; Porezag, D.; Jungnickel, G.; Elsner, J.; Haugk, M.; Frauenheim, T.; Suhai, S.; Seifert, G. *Phys. Rev. B* **1998**, *58*, 7260.
(36) Ohta, Y.; Okamoto, Y.; Page, A. J.; Irle, S.; Morokuma, K. *ACS Nano* **2009**, *3*, 3413.
(37) Aradi, B.; Hourahine, B.; Frauenheim, T. *J. Phys. Chem. A* **2007**, *111*, 5678.
(38) Weinert, M.; Davenport, J. W. *Phys. Rev. B* **1992**, *45*, 13709.
(39) Wentzcovitch, R. M.; Martins, J. L.; Allen, P. B. *Phys. Rev. B* **1992**, *45*, 11372.
(40) Page, A. J.; Ohta, Y.; Irle, S.; Morokuma, K. *Acc. Chem. Res.* **2010**, *43*, 1375.
(41) Page, A. J.; Yamane, H.; Ohta, Y.; Irle, S.; Morokuma, K. *J. Am. Chem. Soc.* **2010**, *132*, 15699.
(42) Swope, W. C.; Andersen, H. C.; Berens, P. H.; Wilson, K. R. *J. Chem. Phys.* **1982**, *76*, 637.
(43) Martyna, G. J.; Klein, M. L.; Tuckerman, M. *J. Chem. Phys.* **1992**, *97*, 2635.
(44) Ohta, Y.; Okamoto, Y.; Irle, S.; Morokuma, K. *Phys. Rev. B* **2009**, *79*, 195415.
(45) Zheng, G.; Witek, H.; Bobadova-Parvanova, P.; Irle, S.; Musaev, D. G.; Prabhakar, R.; Morokuma, K.; Elstner, M.; Kohler, C.; Frauenheim, T. *J. Chem. Theory Comput.* **2007**, *3*, 1349.
(46) Parasuk, V.; Almlöf, J. *J. Chem. Phys.* **1989**, *91*, 1137.
(47) Irle, S.; Zheng, G.; Elstner, M.; Morokuma, K. *Nano Lett.* **2003**, *3*, 1657.
(48) Irle, S.; Zheng, G.; Wang, Z.; Morokuma, K. *J. Phys. Chem. B* **2006**, 14531.
(49) Yamaguchi, Y.; Colombo, L.; Piseri, P.; Ravagnan, L.; Milani, P. *Phys. Rev. B* **2007**, *76*, 134119/1.
(50) Page, A. J.; Yamane, H.; Ohta, Y.; Irle, S.; Morokuma, K. *J. Am. Chem. Soc.* **2010**, *132*, 15699.
(51) Stone, A. J.; Wales, D. J. *Chem. Phys. Lett.* **1986**, *128*, 501.
(52) Karoui, S.; Amara, H.; Bichara, C.; Ducastelle, F. *ACS Nano* **2010**, *4*, 6114.
(53) Ostwald, W. *Z. Phys. Chem.* **1897**, *22*, 289.